Ocean Dynamics (2011) 61:2141–2156
DOI 10.1007/s10236-011-0478-4

Mapping bathymetry using X-band marine radar data recorded from a moving vessel

Paul S. Bell · John C. Osler

Received: 15 March 2011 / Accepted: 19 July 2011 / Published online: 7 August 2011
© Springer-Verlag 2011

Abstract Marine radars mounted on ships can provide remarkable insights into ocean behaviour from distances of several kilometres, placing other in situ observations and the environment around a ship into a wider oceanographic context. It has been known for some time that it is possible to map shallow water bathymetry and currents using radar image sequences recorded from shore based stations. However, a long standing question from military and hydrographic communities has been whether such techniques can be applied to radar data collected by moving vessels. If so, this presents the possibility of mapping large areas of shallow or coastal seas (albeit with a somewhat coarse horizontal resolution of 50–100 m) prior to the surveying vessel actually having to travel into potentially uncharted or dangerous shallow water areas. Trial sets of radar data were recorded by the Canadian Forces Auxiliary Vessel Quest using a Wamos radar digitiser connected to a Decca navigation radar during a number of deployments around Nova Scotia in 2008 and 2009. Georeferencing corrections derived from the existing ship navigation systems were sufficient to allow the application of the existing depth inversion analysis designed for static radar installations. This paper presents the results of bathymetry analyses of two datasets recorded from CFAV Quest while the vessel was travelling at speeds of up to 14 knots. The bathymetry derived from the radar data compare favourably with independent surveys and with the on-board echo sounder to depths of approximately 50 m.

Keywords Bathymetry · Wave inversion · Marine X-band radar · Mapping · Remote sensing

Responsible Editor: Michel Rixen

This article is part of the Topical Collection on *Maritime Rapid Environmental Assessment*

P. S. Bell (✉)
National Oceanography Centre,
Joseph Proudman Building, 6 Brownlow Street,
Liverpool L3 5DA, UK
e-mail: psb@noc.ac.uk

J. C. Osler
Defence Research & Development Canada Atlantic,
Dartmouth, NS, Canada

1 Introduction

The long-term monitoring of any type of ocean area is inherently difficult to perform with in situ instruments due to the harsh environment and the expense of maintaining such equipment. Even from a vessel, only a limited area may be studied; and over the scales on which coastal processes operate, such areas represent little more than point measurements. In contrast, remote sensing techniques are able to view tens of square kilometres of ocean at the same time using equipment mounted on a platform out of the water, improving reliability, power supply options, equipment lifetime and simplifying maintenance.

One of the earliest uses of remote sensing of the ocean dates back to the First World War, during which the British Navy used aerial photographs combined with tidal levels measured from a submarine to map the waterlines of French beaches, allowing contour maps of those beaches to be assembled (Bacon Sir 1932).

Remote beach mapping science was advanced further in the 1940s when analyses of carefully timed aerial photographs were used by the Allied forces to map the Normandy beaches in France in preparation for the D-Day Landings (Hart and Miskin 1945; Williams 1946). The wavelength and celerity (speed) of the waves approaching

the beaches were determined from the photographic sequences and wave theory used to estimate the water depth and hence the beach gradients needed by the Navy for amphibious landings. The technique has been updated in more recent times to take advantage of modern radar and video systems instead of photographs, and computer processing instead of manual analysis, but the principle remains the same.

Imaging radar systems may also be used provided they are capable of resolving the waves. X-band radars are particularly useful in this sense in that their electromagnetic wavelength of 3 cm interacts with the small sea surface capillary waves with wavelengths in the centimetre range through Bragg resonant scattering, generating a detectable backscattered signal that is modulated by the gravity waves with wavelengths from metres to hundreds of metres. This is not the only component of the imaging mechanism of waves by radars at this frequency but a detailed discussion of other imaging effects is beyond the scope of this paper.

A range of radar types use this electromagnetic frequency band, including satellite synthetic aperture radars, satellite altimeters, weather radars and marine navigation radars. The type of ground-based marine radar systems used for the present work are able to generate images of sea surface waves over distances of several kilometres with update rates of approximately 2.5 s as their antennas physically rotate. High-speed versions have a faster rotation time of approximately 1.4 s but are much less common. The wave signatures seen on the radar images are commonly referred to a sea clutter, and are considered noise in most conventional applications of navigation radars.

The radar imaging mechanism of the waves relies on the presence of a minimum amount of sea surface roughness. Hence, even very small waves may be visualised using marine radar on a breezy day with a roughened sea surface, while even a moderate amplitude long period swell on windless day may be completely invisible to the radar due to the lack of any sea surface roughness capable of reflecting the transmitted radar signal back to the transceiver. For this reason, the radar measurement of waves becomes difficult when the significant waveheight falls below H_S=1 m or the wind speed falls below 3 m/s.

Modern deployments of remote sensing systems from coastal stations have allowed the long-term monitoring of waves and sea surface roughness (and hence depth and currents) in adjacent coastal seas using 3D Fast Fourier Transform methods to break down the image spectrum of the waves into discrete components that can be used to determine 2D wave spectra and currents (Young et al. 1985; Senet et al. 2001; Dugan et al. 2001) Commercial systems are now available that build on this and are able to determine calibrated 2D wave spectra and current vectors (Hessner et al. 2008).

Bell (1999) demonstrated a relatively basic analysis on field data from a coastal station in which cross-correlation of image pairs was used to estimate the dominant wave celerity field, and together with the peak wave period this was used to infer water depths using linear wave theory.

If the available radar images are of particularly high-quality, excellent precision in wave parameter determination can be obtained using analysis of wave-phase patterns directly, rather than with spectral methods. Hessner et al. (1999) demonstrated such a technique on data from a radar station on the island of Heligoland in the North Sea. A similar technique was further developed to include filtering of all but a narrow range of wave signals in the DiSC algorithm, thereby further improving the wave-phase measurements (Senet et al. (2008); Flampouris et al. (2008)). It is not clear what range limitations are introduced by the need for high-quality phase patterns in this technique, but excellent accuracy and resolution have been demonstrated at ranges of up to 1 km.

The use of linear wave theory into very shallow water has been found to be an issue by several researchers and approximations to higher-order wave theories that include corrections for higher waves travelling faster than the predictions of linear wave theory have been found to be very effective in mitigating this issue (Holland (2001); Bell et al. (2006); Catalan and Haller (2008)).

Analyses of these derived parameters can provide valuable insights into the behaviour of hydrodynamically and morphodynamically active areas over extended periods of time (Bell 2008, 2009, 2010), although wave inversions are not the only approach for studying such areas using remotely sensed data. Ruessink et al. (2002) demonstrated a technique for observing the increased signals in both video and radar data generated by breaking waves over shore parallel sand bars, and Aarninkhof et al. (2005) used inverse modelling to infer the profile of the bar causing the observed wave breaking. Another approach for intertidal mapping using a waterline method on time averaged radar images was demonstrated on data from the Japanese coast by Takewaka (2005).

Although there are no theoretical reasons why radar sea surface image sequences recorded from a moving vessel may not be used for water depth mapping, prior to this work there had been no opportunity for the authors to collect the required data to test whether practical constraints would be a barrier to this application.

The reasons for wishing to perform depth inversions using data from moving vessels are numerous. While static radar systems are extremely valuable for long-term monitoring of coastal areas, it takes time to get the sites set up, obtain the permissions to transmit from land-based sites and, once set up, the area viewable by the radar is fixed. In contrast, ships often already have suitable radars for safety and navigation purposes, simply requiring a recorder to be

added. In principle, a ship could then map vast areas of coastal seas using radar data collected whilst underway. In addition, for scientific applications, the first requirement for any new study area is a bathymetric map of sufficient accuracy from which to derive model grids and plan equipment deployments, and such data are often unavailable off the shelf, and expensive and time consuming to collect.

Commercially available radar recorders have been fitted to vessels for wave and current monitoring purposes for a number of years. However, the data from these are processed in a different manner to that used in the present study. In the existing applications, the radar image sequences are not required to be georeferenced, other than to record the vessel's average course and speed for the duration of the image sequence. The wave spectra, currents and depths determined are therefore a time and space average for that set of data. Evidently, if the vessel is travelling at any significant speed, the waves sampled by the radar images are likely to be aliased in time. However, the effect of aliasing on the location of the wave energy within the image spectrum is well documented (Senet et al. 2008), may be accounted for, and the correct mean water current and wave spectra can still be determined.

In the present study, the lack of image georeferencing of the existing technique is undesirable because the waves are no longer assumed to be homogeneous over the imaged area, but rather are assumed to be influenced by the underlying bathymetry at significantly finer spatial scales. It is therefore necessary to georeference every radar image and produce sequences of radar images in which each pixel time series in the image sequence corresponds to a fixed point in space rather than one in which the instantaneous pixel locations move with the motion of the vessel. This should remove the vessel motion from the resulting image sequences at the start, and thus aliasing of the wave signals due to high vessel speeds should not be an issue. Hence, the aim was to ensure that the wave behaviour corresponding to a specific area of the sea bed could be analysed to extract the local water depth, as would be the case for a radar sited on a fixed platform. The analysis is based on the commonly used 3D FFT approach, augmented by a technique to more accurately identify spectral peaks with low wavenumbers in the spectrum that provides additional information to assist fitting the wave dispersion equations in deeper waters.

The aim of this work was to acquire a number of radar image sequences and test whether the data from existing navigation instruments were sufficient to allow georeferencing of the radar images with an accuracy suitable for depth mapping using algorithms that are already in use for radars at fixed locations. The region of applicability of this technique is discussed in relation to wave theory and radar capabilities, and the techniques used to georeference the radar images and extract the required wave information are described. Data recorded from two coastal areas of Nova Scotia were collected from the CFAV Quest whilst underway and the results of the depth inversion analysis are presented and compared with gridded bathymetry data collected using conventional survey methods.

2 Depth inversions

The depth inversion technique uses the relationship between water depth, wave period and wavelength, known as the wave dispersion relationship, to identify the water depth given the wavelength and period. This is possible because the effects of waves do not simply propagate on the water surface, but penetrate down through the water to depths proportional to their wavelength. The presence of the sea bed or a current within that depth of influence will alter the way the waves propagate in a measurable way.

The principle of this technique is to measure the wave propagation characteristics and use those to infer the most likely conditions that led to that wave behaviour. The specific property that waves exhibit in this sense is that they slow down and the wavelength gets shorter as they travel into shallower water. Conversely, if waves propagate from shallow water to deeper water they speed up and the wavelength increases. Any technology capable of imaging that change in wave behaviour may therefore be used for this purpose.

There are various methods of mapping the desired wave properties of wavelength and period from such data. If the wave patterns imaged by the radar are clear and easily discerned, one can even measure the wavelengths manually from plots (Heathershaw et al. 1980). Wave patterns with a broad spectrum of wave periods and directions are more complicated to analyse and require spectral analysis methods to separate and measure the respective wave properties.

Spectral analysis using Fourier analysis techniques transforms the problem from the 3D time–space domain into the 3D frequency–wavenumber domain. In frequency–wavenumber space, the energy of the waves propagating in a given water depth would be found clustered around a 3D surface that resembles a flared cone, the exact shape of which is defined by the wave dispersion relationship for that water depth. If enough wave components are present at a range of wave periods and directions to identify that cone shape in frequency–wavenumber space, a wave dispersion surface can be fitted to the measured wave components, the parameters of which identify the water depth with a considerable degree of certainty. In reality, waves often come from a narrow band of directions and frequencies, and so

instead of the wave components outlining the complete cone shape of the dispersion surface, they are clustered around a small part of that surface and the fitting exercise becomes a task similar to estimating the shape and size of a prehistoric pot based on a small fragment of pottery. The wider the directional spread of the wave components and the broader the frequency distribution of the waves, the more reliable becomes the fitting procedure.

2.1 Region of applicability of depth inversions

The derivation of water depth from wave behaviour is inherently limited to waves that are influenced by that water depth in a measurable way. The value of this depth limit varies as it depends on the site and the waves present at any particular time.

Text books often quote that waves begin to 'feel the bottom' when the depth is less than half their wavelength, a point where the wavelength is within 99.5% of the deep-water wavelength. Trying to measure differences in water depth using waves close to this threshold is simply unrealistic as a large change in water depth gives rise to only a very small change in wavelength.

A more practical limit for this type of work would be to say that the waves may be used for mapping water depth if their wavelength is less than approximately 90% of their deep-water wavelength, or the depth of approximately a quarter of the wavelength. This can be illustrated by plotting the wavelength (according to linear wave theory) of a variety of wave periods over a range of depths as shown in Fig. 1.

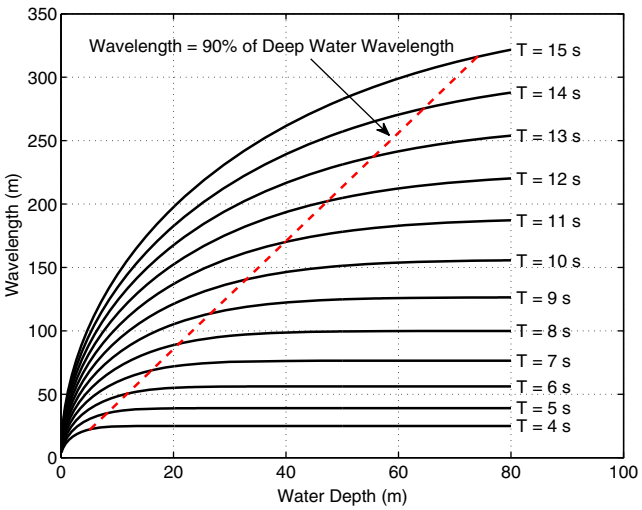

Fig. 1 Wavelength vs water depth according to linear wave theory for wave periods of 4–15 s. The *dotted line* marks the threshold where the wavelength equals 90% of the deep-water wavelength and is an approximate guide to the practical depth limit of depth inversions

The deep-water wavelength according to linear wave theory (Airy 1845) is

$$L_0 = \frac{gT^2}{2\pi} \tag{1}$$

Where wave period = T

Linear theory wavelength

$$L = L_0 \tanh kd \tag{2}$$

Where wavenumber $k = \frac{2\pi}{L}$, and depth = d

The threshold line of L=0.9L_0 has been overlaid on the curves depicting linear wave theory in Fig. 1 and can be considered as a reasonable rule of thumb for the maximum depth likely to be able to be detected for a given set of waves. To the left of the line, the wavelengths vary sufficiently with water depth to be useful while to the right of the line, changes in water depth have little effect.

For example, in Liverpool Bay in the United Kingdom, the limited fetch afforded by the sheltered nature of the Irish Sea means that the longest period waves likely to be experienced are around 7–8 s. According to Fig. 1, such waves would enable depths of no more than 15-20 m to be detected, and this is found to be the case in practice. However, on an open coastline such as that of the Atlantic coast of Nova Scotia or the east coast of the USA where long period swells of 12 s or higher would not be unusual, one might reasonably expect to detect water depths down to 50 m or more. Beyond this depth limit, a depth inversion analysis will tend to 'bottom out' to that depth limit because the waves will travel little faster and have little further increase in wavelength no matter how much deeper the water becomes.

2.2 Non-linear wave dispersion equations

Although linear wave theory works well for many applications, it slightly underestimates the wave celerity and hence wavelength of larger amplitude waves. For wave inversion applications this means that water depths tend to be slightly overestimated, an effect that is particularly significant in terms of percentage error in very shallow water close to the shore.

Instead, a dispersion equation that approximates the behaviour of higher-order wave theories has been adopted. This dispersion equation is based on linear theory but with a correction for amplitude dispersion, i. e. the non-linear behaviour of large waves in shallow water which travel faster than linear theory alone can predict (Hedges 1976). There is also a correction for

currents to account for the Doppler shift of the waves travelling on a mean current:

Wavelength according to Hedges (1976):

$$L = \frac{2\pi g \tanh k(d+Z)}{(\omega - \mathbf{k}.\mathbf{U})^2} \quad (3)$$

where angular frequency $\omega=2\pi f$ and $\mathbf{U}$ is a mean current vector.

Amplitude dispersion correction factor $Z=0.5H$ (Booij 1981), or $Z=0.35H_S$ for spectral waves

H = wave height, H_S = significant wave height

Equation 3 can be easily rearranged for water depth

$$d = \frac{1}{k}\left(\tanh^{-1}\frac{(\omega - \mathbf{k}.\mathbf{U})^2}{gk}\right) - Z \quad (4)$$

The difference that the amplitude dispersion correction makes to the results of a depth inversion was studied in a field trial (Bell et al. 2006) using the combination of a marine X-band radar and a 77-GHz high-resolution radar that allowed wave propagation to be followed right into the swash zone on a beach in Portugal. Linear wave theory was consistently found to overestimate the water depth, while the approximation based on Hedges' equation reproduced the water depths right up to the waterline with remarkable accuracy.

There are numerous other possible approximations that more accurately reproduce the nuances of higher-order wave theory (e.g. Kirby and Dalrymple 1986; Hedges 1987; Kirby and Dalrymple 1987) but the water depths calculated by the various equations have been studied in a large wave flume and have little to choose between them in practice. This is because the error bounds involved in measuring the inputs to the equations in terms of wavelength, period and height tend to exceed the differences between the depths due the various equations (Catalan and Haller 2008), so there is little to be gained by using any but the simplest of these approximations to non-linear wave behaviour.

Marine radar wave height determination involves the empirical calibration of modulation transfer functions for each radar setup, and numerous studies indicate that these can be quite effective. The calculation of wave height directly from the radar data as a varying quantity for use in Eq. 3 was beyond the scope of the present study. Instead, in order to simplify the analysis, a single wave height measured from the ship was assumed as a constant value for each trial.

3 Data collection

The aim of the trials described was to demonstrate whether wave inversions could be used to map bathymetry using data collected on an opportunistic basis from a moving vessel using a radar recorder, in this case a Wamos system (Reichert et al. 1998), together with the ship's standard navigation system data for georeferencing.

Two sets of data were collected with different recording regimes. The course followed by the ship on each occasion is marked on the map in Fig. 2. The first dataset was recorded on 20th March 2008 while CFAV Quest was on approach to Halifax, Nova Scotia. It comprised a single record spanning approximately 20 min and containing 512 radar images with a radial range of 2 km and a radial sampling distance of 7.5 m corresponding to a sampling rate of 20 MHz. The software version of the Wamos digitisation system at that time recorded only the start time and average rotation rate of the radar antenna. The ship's navigation data were recorded separately at 10-s intervals, providing a position and bearing fix approximately once every four radar images. The significant waveheight was measured by an on-board system as 1.4 m.

The second set of data was collected on 6th November 2009 in St Margaret's Bay, located approximately 30 km west of Halifax. St Margaret's Bay is an enclosed rocky bay approximately 12 km in length and varying in width from 4 km at the mouth to around 8 km further into the bay. These data conformed to the standard sampling regime of the Wamos used for wave monitoring and comprised multiple sets of 32 radar images spanning around 70 s each, usually separated in start time by 2 min. The Wamos recording software was upgraded prior to this dataset to allow each frame to be time-stamped and contain a bearing from the ship's gyroscope. Position data from the GPS system were recorded every 2 s. Significant waveheight was measured as 2.1 m.

The survey data used for comparisons were collected by the Canadian Hydrographic Service and were compiled from a number of surveys. These data were median gridded to a spacing equivalent to that of the radar bathymetry output.

4 Analysis

4.1 Image georeferencing

For both datasets the aim was to plot each radar image centred on the position of the ship at the moment of recording and rotated to the bearing recorded by the ship's gyroscope relative to true north, thus nominally placing the radar images in their correct geographic position. In order to simplify this process, the ship was assumed to be static for the 2.3 s it took to build up each image as the radar antenna rotated. While it would be theoretically more accurate to georeference each individual radar pulse to

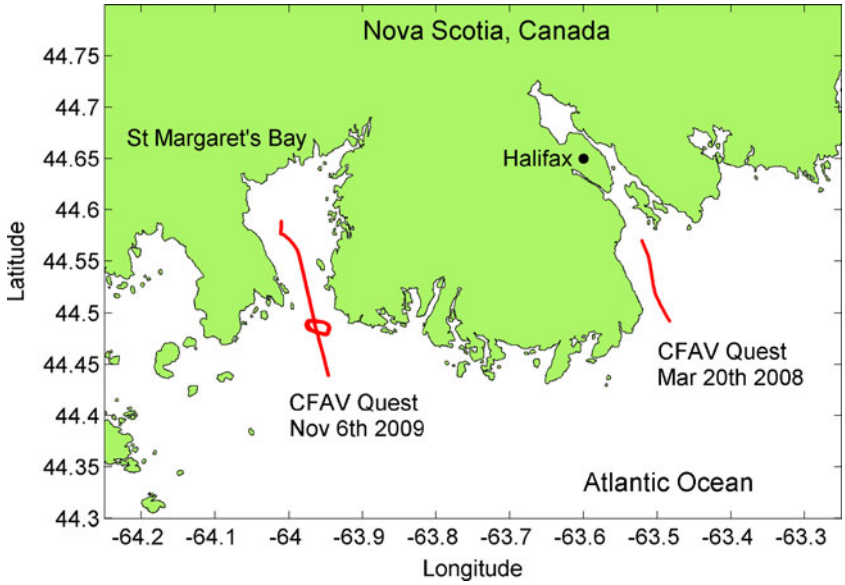

Fig. 2 A map of the study areas in the waters approaching Halifax, Nova Scotia and St Margaret's Bay. The course of the CFAV Quest during the recording of the two sets of radar data is marked in *red*

account for the continuous change in ship position and orientation, the accuracy and update rate of the georeferencing data was considered insufficient to warrant the considerable additional processing this would require.

Prior to addressing the georeferencing aspects of the image sequence, the range dependency of the background radar signal was removed by finding the mean of all the radar backscatter radials and subtracting that mean background from each pulse in the polar images. This is a simple but effective method of creating radar images that contain a zero-mean variation in radar backscatter, and generates more consistent image sequences than using raw images alone.

4.2 Halifax approaches

During the dataset recorded on approach to Halifax, the ship's navigation data were recorded separately at 10-s intervals, providing a position and bearing fix approximately once every four radar images. The speed of the CFAV Quest varied between 10 and 14 knots during the recording of the radar sequence, hence the ship would have travelled 50–70 m between position and bearing fixes.

The software version of the Wamos digitisation system at that time was an early version that recorded only the start time of the image sequence and the rotation rate of the radar antenna. Therefore, in order to georeference each radar frame, the navigation data were initially interpolated to the calculated time of each radar frame based on the start time and assuming a uniform radar antenna rotation rate.

Unfortunately, it quickly became clear that the radar antenna rotation rate was not sufficiently stable to allow the image positions and orientations to be determined in that manner. Using the assumed time, and hence position and orientation of the radar frames, led to fixed targets drifting in apparent position from frame to frame, precluding precise analysis of wave propagation from the radar data, particularly for long radar records as in this case.

This is a subtle effect that would be unnoticeable for the standard navigation applications for which radars are manufactured and is common to all radars so far used by the author for wave analysis.

In order to more precisely identify the recording time of each radar frame and hence more accurately relate the radar images to the navigation data, a proxy of the ship's variation in bearing was derived from the wave directional information in each radar image. The assumption was made that during the time taken between any two radar frames (approximately 2.3 s), the waves recorded within the radar images should not alter their directional characteristics in any statistically significant way. Therefore, a cross-correlation in terms of bearing of the directional wave spectra of any two successive frames should demonstrate a lag in bearing corresponding to the rate of turn of the ship. This analogue of the ship's rate of turn could then be compared with the known rate of change of bearing calculated by taking the derivative of the ship's gyroscope data which were recorded together with the GPS time and position fix.

Initially, the rate of turn of the ship at the time of each frame was calculated based on a steady radar antenna rotation rate and the start time of the record. The rate of change in bearing is plotted in Fig. 3 as the solid line. Overlaid on that is the proxy of that signal derived by cross correlating the individual radar image spectra from one frame to the next in terms of bearing. Although the signal

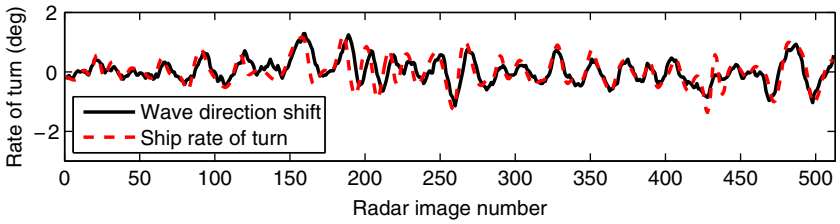

Fig. 3 The rate of change of the ship's bearing derived from the angular change in the 2D wave spectra of successive radar images is plotted as the *red dotted line*. The ship's gyroscope interpolated to the assumed radar image times is plotted in *black*. The timing discrepancies are clear, particularly around image 200

derived from the wave spectra is very similar to that derived from the gyroscope data there is clearly a slowly varying discrepancy in time between the two records.

This time discrepancy was identified using a simple matching algorithm that minimised the lag between the two records using a moving window with a width of 60 frames. The time lag found by this method is plotted in Fig. 4 in seconds.

The calculated lag was then used to correct the estimated recording time of each radar frame, and the position and bearing for each frame were recalculated. The initial and the corrected ship bearing for each radar frame are shown in Fig. 5, and the difference between them is plotted in Fig. 6.

These errors in bearing exceed 4° in places, and it is worth noting that a 1° error in bearing at a range of 2 km gives rise to an error in horizontal coordinates of 35 m. Errors of several degrees therefore have a profound effect on the accuracy of the image georeferencing. For example, a 2° error would displace the radar echo by 70 m at a range of 2 km, which is approximately half the wavelength of a 10-s wave, or a full wavelength of a 7-s wave travelling in 40–50 m of water. The determination of wave propagation measurements while such positioning errors are present is unlikely to be successful.

The differential of the final calculated bearing signal (rate of turn of the ship) has been overlaid onto the analogous signal derived from the wave spectra in Fig. 7, and the two signals no longer exhibit any visual evidence of time discrepancies.

The correction of the radar image recording times allowed the georeferencing accuracy of the radar images to be improved sufficiently such that fixed targets no longer appear to drift in position, although a small jitter in their bearing and position could still be observed. This jitter was also observed in the St Margaret's Bay dataset that had frame by frame gyroscope, time and hence position stamps and is therefore thought to be a result of the simplifying assumption that the ship can be considered as a static platform within the time period required to record a single frame. There may also be small errors introduced from the pitch and roll of the ship influencing the look-direction of the radar beam. Such errors could, in the future, be corrected by using the data from commercially available high-resolution position and orientation systems (Hill 2005).

The approach of using the wave signals contained within the recorded data to assist in stabilising the georeferencing of the data may have wider applications, particularly in stabilising video image sequences recorded from the increasing variety of small remote controlled aeroplanes being used by the research community. Analysis of the wave patterns visible in the images could provide extra information that would help stabilise georeferencing in the absence of fixed reference points within the images.

The finite time taken for the radar antenna to sweep through 360° to build up a single image introduces a further error to the calculated time of individual pixels, but one for which at least a first-order correction is possible. The antenna rotation generally has minimal effect on data recorded from a static platform, but can introduce a variation in the time taken to record successive pixels from a moving platform as the ship changes position and

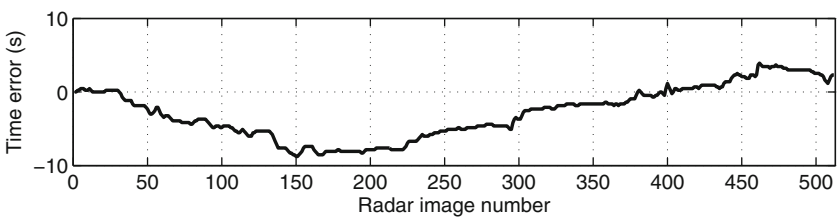

Fig. 4 The time difference between the assumed image time and the image time derived from lag between the rate of turn calculated from the ship's gyroscope and frame to frame shift in apparent wave direction calculated from the 2D wave spectra analysis

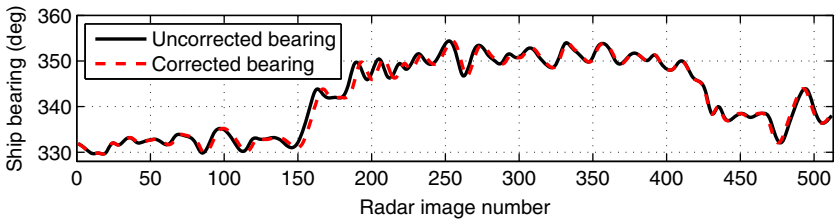

Fig. 5 The bearing relative to true north for each radar frame before correction (*black solid line*) and after correction using the wave spectra information to adjust the image time (*red dashed line*). The differences around image 150–200 are clear

bearing. To correct for this particular source of error, an additional time correction was calculated to estimate the actual time of recording of each radar pixel in each radar frame based on the start time of each image and the difference in angle between the start bearing of the radar image and the bearing of the pixel location. This difference in bearing then gives the fraction of the radar antenna rotation time to include as an offset to the start time of the radar frame. The result of this is a time series of the radar signal for each pixel, with an unsteady sampling rate. The time series for each pixel location was then simply interpolated to a steady sample interval corresponding to the average antenna rotation rate, resulting in a radar image sequence with uniform time intervals and in which all the pixels in a particular image correspond to the same instant in time.

4.3 St Margaret's Bay

Following the complexity of the corrections required to georeference the Halifax radar data, the operating software of the Wamos was upgraded to allow frame by frame gyroscope and time stamps to be recorded within the radar records. This dispensed with the need to use the wave signals to assist in the georeferencing.

Another difference from the Halifax trial was that instead of the single long record of 512 images, the sampling regime followed the default settings used for standard wave sampling of 32 images per record. This provided multiple short records of 74 s beginning at 2 or 3-min intervals. Although short records such as this can produce adequate bathymetry results when recorded from static radar installations, the results from this bathymetry analysis proved noisy. To overcome this, several short sequences were stitched together to create longer records of 256 images spanning just under 10 min each. Blank images were inserted between the records, and the timestamps provided the time reference to allow the accurate temporal alignment of the records. In all other respects, the analysis followed the same approach as the Halifax trial.

4.4 Bathymetry inversion

The principle of the bathymetry inversion is to fit the wave dispersion relationship that relates water depth to wave period and wavelength or wavenumber to the observed wave behaviour within the radar image sequences. For the Halifax trial the fact that the ship was moving relatively quickly meant that although the radar record comprised 512 images in total, less than half of those images contained radar data for any particular geographic position as the 'dwell time' of the radar recording footprint was less than half the total record length. Therefore, for the main section of the depth inversion analysis the analysis area was split into tiles of 1–2 km^2 and only a 256-image window centred on the time period actually containing data in each tile was analysed.

Under ideal conditions, with a fixed platform for the antenna and where waves at a range of frequencies give clearly defined patterns within radar data, it is possible to derive remarkably high-resolution bathymetry data from these remotely sensed images using relatively small analysis windows of around 100 m square (Bell 2010). Unfortunately, such ideal conditions are rarely found when they are wanted in the field, and the recorded data often show poorly defined wave patterns that require relatively large areas to be considered before the desired wave signals emerge above the noise floor. The use of a moving platform

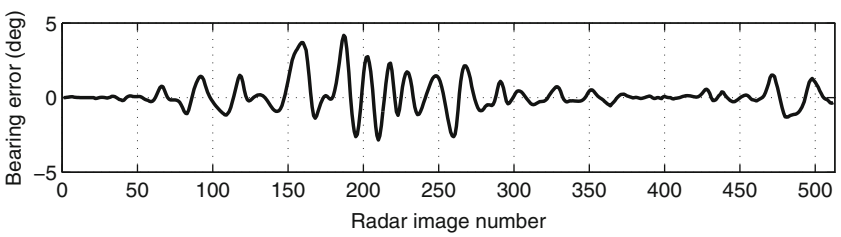

Fig. 6 The bearing error caused for each radar image by assuming a uniform interval between radar images

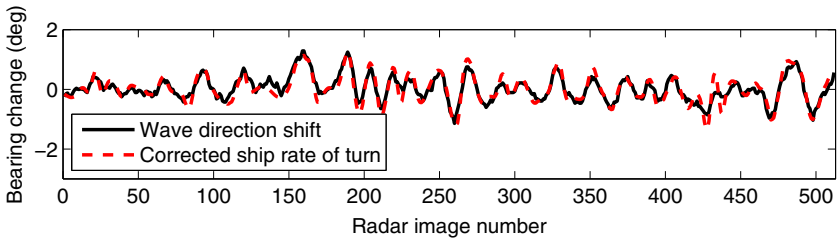

Fig. 7 The corrected rate of turn of the ship for each radar frame (*red dashed line*) overlaid on the apparent change in wave direction determined from successive radar image spectra. The two signals overlay perfectly now, indicating the timing of the radar frames is accurate

with imperfect georeferencing of the radar images further reduces the ability of analysis techniques to extract the wave signals. In the present study using the Halifax data, it was found necessary to use a particularly coarse analysis window of 640 m square to obtain reasonable quality results, translated at a quarter of that window size, i.e. 160 m. The St Margaret's Bay data proved slightly better quality and a window size of 480 m translated at 120 m intervals was found to be acceptable. This finite window size leads to an inherent smoothing of the detected bathymetry corresponding to the size of the analysis window.

At each analysis window position, the following procedure was carried out: a 3D Fast Fourier Transform (FFT) was applied to the selected data window yielding a 3D frequency–wavenumber spectrum (Young et al. 1985). This was performed by first carrying out a 1D FFT in the time domain of the image sequence yielding complex single-frequency image (CSFI) components (Bell 1999). An example of a series of such CSFIs from a single analysis tile from the Halifax trial is shown in Fig. 8. The wave patterns corresponding to the individual wave periods have been visualised by plotting the real component of the CSFIs and as expected can be seen to reduce in wavelength as the wave period reduces. The wave periods shown in Fig. 8 correspond to those Fourier components in which coherent wave patterns could be identified by eye, starting with periods of 13 s, appearing most strongly in the 9–10-s band and fading away again at around 8 s. The lack of identifiable wave patterns in the sub 8-s band is thought to be a result of the insufficient accuracy of the image georeferencing. Records from static platforms generally exhibit very clear wave patterns in the sub 8-s spectral region. The appearance of discernable wave patterns with wave periods up to 13 s suggests from Fig. 1 that the maximum depth detectable should be approximately 50 m for this dataset.

These single-frequency complex images are then passed through a 2D FFT to determine the 2D wavenumber spectra for each wave frequency.

The highest amplitude signals within those spectra are assumed to correspond to the ocean waves, and a wave dispersion surface was fitted to those frequency–wavenumber combinations by maximising the value of the spectral intensities on the dispersion surface, yielding an estimate of the water depth and, if selected, a current vector.

During initial analysis runs, an attempt was made to determine both depths and currents using these data. However, the determination of both parameters was found to substantially increase the noise level in the results without dramatically altering the resulting depth patterns. Further investigation suggested that the remaining jitter in the georeferencing of the images was degrading the ability of the 3D FFT to isolate the higher frequency wave components that are most sensitive to the currents. As a result, it was decided to turn off that aspect of the analysis and assume no current. The dispersion fit has also been limited to waves that are a few frequency bins lower than those in which waves can be seen visually for the same reason—a wave period cut-off chosen to be 6 s. Further work may enable this aspect of the data analysis to be revisited at a later date.

In terms of computational effort, the single Halifax record was able to be processed using Matlab running on a 3-year-old laptop with a 2-GHz processor in approximately 2 h. The St Margaret's Bay data comprised multiple records and it took 1–2 days of processing time to run through them all. It is anticipated that substantial savings in computation time could be achieved with the advent of multicore graphics card processing and efficiency improvements in the author's programming of the algorithms.

4.5 Localising low wavenumber components

The initial 1D FFT carried out through the time domain separates out the wave frequency spectrum into the CSFI layers. The sequences of 256 images, i.e. time series of approximately 5 min duration are adequate for this purpose. It is then necessary to determine the 2D wavelength or wavenumber spectrum of each wave frequency component. For pure sinusoidal waveform

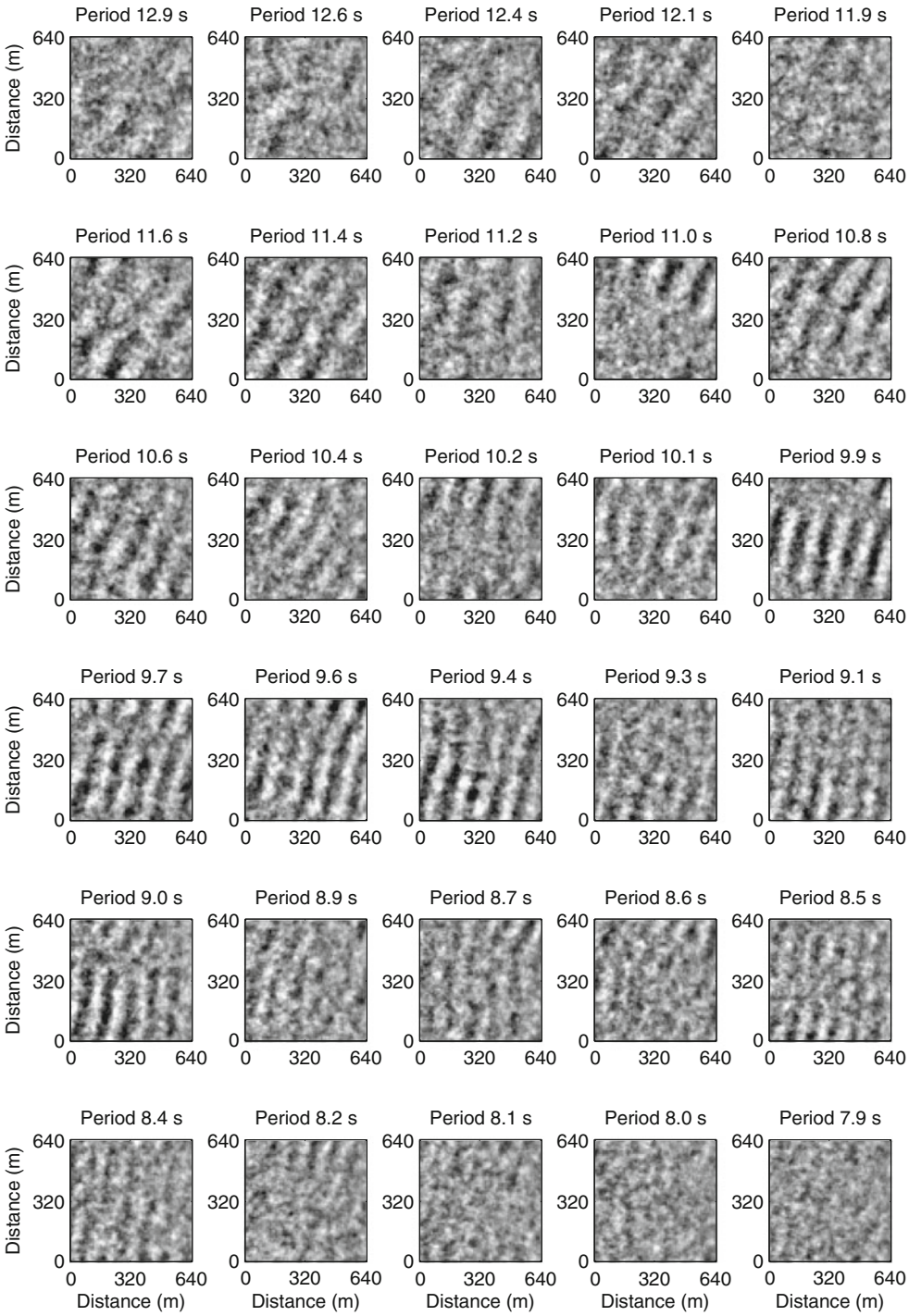

Fig. 8 The real component of a set of complex single-frequency images of waves from a single analysis tile in the Halifax dataset. The change in wavelength through the wave periods is evident

data, this could be achieved with as little as the adjacent pixels. For more realistic data with poor signal to noise levels, a larger area of the sea must be analysed using a 2D Fourier analysis to yield a 2D spectrum of wavenumber components.

The FFT algorithm provides estimates of the energy contained in discrete integer wavenumber intervals. For signals that contain a large number of waves in the data window, this is unlikely to be a problem. However, for physical data windows in which there are a relatively low number of long wavelength waves, i.e. low wavenumber components, the accuracy of the wavenumber (and hence the wavelength) estimation is inherently poor. This is particularly unfortunate for this application since as can be seen in Fig. 1, the maximum depth that can be felt by the waves increases with the wavelength of the waves, and where small errors in wavelength estimation can generate large errors in derived water depth.

For example, in Fig. 8 it can be seen that the waves just visible in the 12.9-s CSFI are of a length that allows three to four waves within the analysis window. The depth indicated by there being three waves in a 640 m window (213 m wavelength waves) is approximately 40 m, while the presence of four waves in the 640 m window (160 m wavelength) would indicate a depth of less than 20 m. This degree of localisation of the spectral peak in wavelengths is likely to be of relatively little help in accurately determining the water depth with any certainty in deeper waters, hence the need for an algorithm that will give a more accurate wavenumber (and hence wavelength) determination for this application.

There are a number of existing approaches to picking out the precise peak in an FFT spectrum. One approach is to zero-pad the ends of the data to increase the wavenumber resolution (Bendat and Piersol 1971). However, in order to substantially increase the accuracy at very low wavenumbers one would have to zero-pad to a substantial degree, and even then the answers would inherently be confined to discrete wavenumber values rather than a continuum of possibilities. Another approach is to fit a parabola through the spectral peak and the two values either side of the peak, from which the peak in the parabola and hence the peak in the spectra can be estimated more closely than the FFT alone.

To identify the precise location of the peak wavenumber component in any 1D or 2D complex signal, a spectral peak localisation method was developed, loosely modelled on the phase locked loop (PLL; Banerjee 2006) used for many years in FM radio receiver tuning. In the phase locked loop electronic circuit, an incoming waveform (e.g. an FM radio signal) is compared in phase with a reference frequency close to that of the incoming signal. The phase error between the incoming signal and the reference is used to apply a correction to the reference signal's frequency to bring it into agreement with that of the incoming waveform. In the example of FM radio, the varying voltage used to control the reference signal is used to recreate the analogue audio information for that radio channel.

The analogy with the FFT follows that the FFT basis functions provide discrete values of the reference frequency, whereas what is desired is a continuum of reference frequencies capable of tracking signals at all relevant frequencies. The closest discrete basis function can be thought of as the PLL reference signal that is not an exact match with the waveform being analysed. If a phase error signal between that basis (reference) function and the signal can be derived, it is a simple matter to determine the frequency that the basis function ought to have to if it were to be an exact match to the signal.

In one dimension, the algorithm works as follows. A standard 1D FFT is performed on a complex signal that is assumed to be homogeneous in space. The peak of the FFT spectrum is identified and a complex waveform corresponding to that spectral component recreated by zeroing all other spectral components and using an inverse FFT. That recreated signal is unlikely to be an exact match to the dominant waveform in the signal, so the phase error between the two signals is determined on a point by point basis by simply performing a complex division between the two signals. If the two signals are not a precise match, the array of phase errors should exhibit a linear relationship to which a straight line can be fitted, the gradient of which supplies the correction to the basis function frequency needed to provide a best match with the original signal. The mean modulus of the result provides a scaling factor that indicates how much larger the actual peak signal is compared with that of the FFT peak, and hence providing a way of determining the amplitude of the fitted signal.

The process is illustrated by the flow chart in Fig. 9. Extension to two dimensions is then a straightforward exercise allowing 2D signals to be analysed for the precise spectral peak.

For example, let us create a complex waveform $\eta(x)$ of amplitude = 1 made up of $n=64$ values comprising 3.55 waves and an arbitrary phase. Figure 10a shows this waveform, the real component plotted in red and the imaginary component in blue.

The FFT of that signal shows a peak wavenumber at 4 waves, but with significant energy at 3 waves, as one might expect. Recreating the signal of that spectral peak by nulling all other components and using the inverse FFT gives the signal in Fig. 10b. The differences between the original signal and that of the waveform representing the peak of the spectrum are evident in the shorter wavelength and smaller amplitude of the recreated signal.

In complex mathematics, if one divides one complex number by another, the argument of the answer indicates the phase difference between the two numbers, and the modulus give the ratio of the magnitudes of the two signals. Hence, by dividing the original signal by the peak FFT basis (reference) signal and taking the argument (phase) of the complex result, the phase differences (errors) $\varepsilon_{\text{phase}}$ at each point in the time series are obtained, and are plotted in Fig. 10c. Then a straight line is fitted to this phase error signal, the gradient of which indicates the correction required to the rate of change of phase of the basis waveform in order to bring it into agreement with the original signal. In addition, the mean modulus indicates how much larger the original signal is compared with the reconstructed peak of the FFT—referred to here as the PLL scale factor.

In this example, the gradient was calculated as −0.044179, and the mean of the modulus of that phase

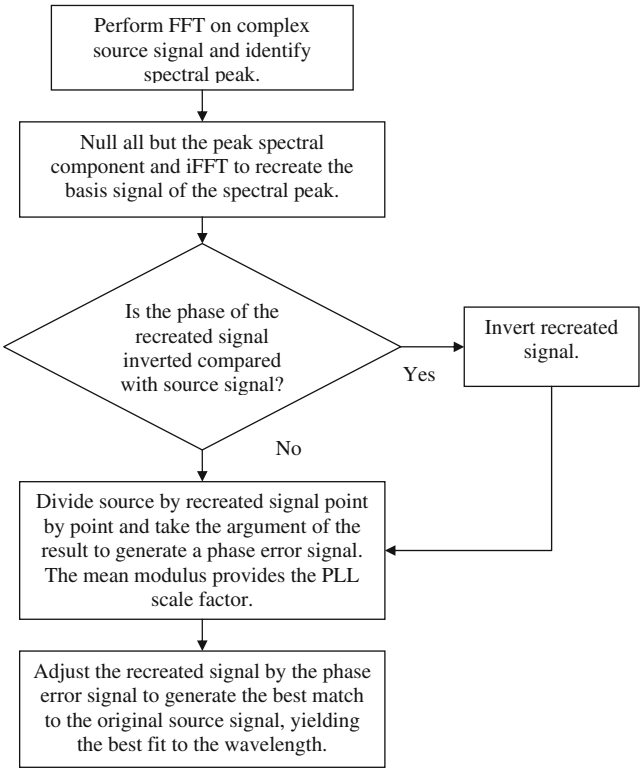

Fig. 9 Flow diagram of the Phase Locked Loop based algorithm to find the spectral peak in complex data

error signal gives a PLL scale factor of 1.4312. Hence, when originally synthesised, the waveform comprised 3.55 waves in 64 samples, i.e. a wavelength of 18.03 samples. The wavenumber peak of the FFT spectrum was located at 4 waves in 64 samples, i.e. a wavelength of 16 samples and with an amplitude of 0.6987.

The calculated peak wavenumber in the spectrum using the phase error as a correction factor is thus:

$$k_{\mathrm{PLL}} = k_{\mathrm{FFTPeak}} + \frac{d\varepsilon_{\mathrm{phase}}}{dx}\frac{n}{2\pi} = 4 + (-0.044179)\frac{64}{2\pi}$$
$$= 3.55$$

Where k_{PLL} is the PLL spectral peak and k_{FFTPeak} is the FFT spectral peak

The amplitude of the PLL spectral peak is simply determined by multiplying the amplitude of the FFT spectral peak by the PLL scale factor.

The PLL derived peak wavenumber and amplitude are all that are required in the present application to augment the standard FFT spectral information in the wave dispersion fit. However, if desired the best estimate of the original waveform may be reconstructed for comparison. This has been plotted in Fig. 10d and is an excellent match with the original waveform in Fig. 10a.

The standard FFT amplitude spectrum has been plotted in Fig. 10e as the black asterisks, and the peak of the spectrum identified by the above method added as the red circle. As expected, the calculated spectral peak can be seen to fall between two standard FFT spectral estimates and have greater amplitude.

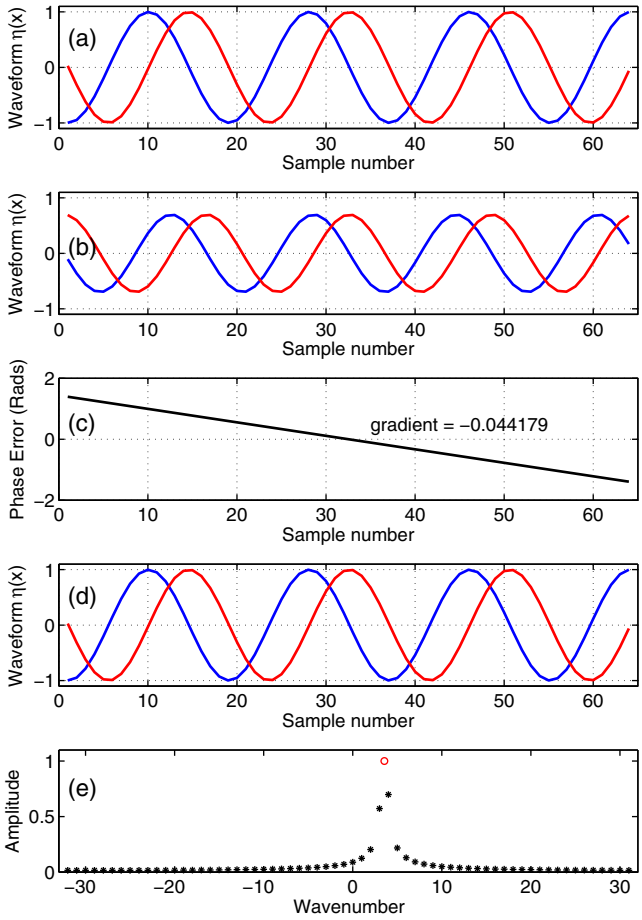

Fig. 10 **a** Complex test signal with 3.55 waves in 64 samples. The real component is plotted in *red* and the imaginary in *blue*. **b** The recreated signal of the spectral peak in the standard FFT. **c** The phase error between original and recreated signal. **d** The recreated spectral peak signal following adjustment by the phase error signal. **e** The standard FFT amplitude spectrum plotted as *black asterisks* with the peak identified with the PLL-based algorithm as the *red circle*

This 1D algorithm is easily extended to 2D complex data although care must be taken when one of the wavenumber components is less than one as this represents a wavelength component longer than the length of the supplied data. This can result in the inverse FFT step of the algorithm producing a waveform that is inverted compared with the synthesised waveform, potentially resulting in discontinuities in the phase error signal and problems fitting a line to it. This issue is easily tested for in the algorithm and the reconstructed basis function can be inverted if necessary. Note that wavenumber components that fall almost perpendicular to the wave direction can easily fall into that category.

In the present application, this algorithm works in tandem with the standard FFT and uses as an input the relevant CSFI generated by the initial 1D FFT of each pixel time series described above. After the 2D FFT of each CSFI has been performed as part of the standard 3D FFT algorithm, the strongest wavenumber component is identified for that CSFI. The algorithm described above then gives the precise wavenumber and amplitude of the spectral peak for that particular wave period, and not limited to the discrete integer wavenumbers inherent in the standard FFT. The strongest signal in the CSFI is identified even if there is little coherent pattern in the CSFI, but as with the standard 3D FFT spectrum, components with poor coherence and small amplitude contribute little to the overall depth fit which works by maximising the spectral energy values on the dispersion surface.

The peak wavenumbers generated by this method augment the results of the conventional 3D FFT in the dispersion equation fit and are aimed at improving the accuracy of the water depth determination in deeper waters where the most useful wave components are those with the longest wavelengths and lowest wavenumbers that penetrate deepest through the water column.

5 Results

5.1 Halifax

The depth inversion of the ~20-min Halifax radar record is shown in Fig. 11 in Universal Transverse Mercator coordinates. The colour scale indicates depth, and the coastline data plotted in black were obtained from the USGS Coastline Extractor hosted on the NOAA website.

Comparison survey data, relative to chart datum (LLWLT), from the Canadian Hydrographic Service were median gridded to the same grid as the radar analysis output. The tidal level was determined from the mean difference between the CFAV Quest's echo sounder record and the survey and found to be a consistent cluster of values with a mean of 2.3 m. Figure 12 shows the survey data with that tidal offset of 2.3 m added.

Figures 11 and 12 show remarkably good correlation considering the radar-derived map was based on less than 20 min of data with imperfect georeferencing. Figure 13 shows a plot of the direct comparison between the survey and radar data. The radar-derived depths can be seen to lose their correlation with the survey at around 50 m as expected, but for waters within the applicable range of this technique there is negligible offset and a reasonable quantitative correlation of 0.9, giving an R^2 value of 0.82.

In the shallowest waters, the radar-derived depths appear to be over estimating the water depth. However, if the survey plot is inspected, it can be seen that the shallowest depths span relatively few pixels and are surrounded by deeper water. The reason for the bias in the result in shallower depths is thought to be that the radar-derived depths are actually based on an area with four times the physical dimensions of the output grid, so the results will be biased to the mean of that analysis area and may well miss the shallowest areas if they make up only a small proportion of the analysis window.

5.2 St Margaret's Bay

The combined depth inversion data from all of the records from St Margaret's Bay is shown in Fig. 14. The data on which these data are based were collected over a 2 hour period around low water in St Margaret's Bay between 19:50 UTC and 21:00 UTC.

The tide prediction for Boutiliers Point in the north of St Margaret's Bay was 2.1 m at 13:58 UTC and 0.3 m at 20:54 UTC. Since the data span a period from around 19:00–21:00 UTC, as a minimum there ought to be a 0.3–0.4 m predicted tide level added to the survey. In addition, with the storm blowing onshore showing a significant waveheight of 2.3 m, it would not be unreasonable to expect an additional surge of a metre or more. An attempt was made to empirically find the tidal offset using the same approach as with the Halifax data by determining the offset between the CFAV Quest's echo sounder and the survey data; however, the results were not nearly as consistent as with Halifax approaches with no easily discernable pattern. This is thought to be due to a combination of factors including the large geographical area covered, the variability within that area, the 2-h duration of the trial and the effects of the storm. As a result, no tidal correction has been applied to the survey data and it is plotted relative to chart datum in Fig. 15.

Without a tidal correction, the radar-derived depths consistently show deeper waters than the survey, by a mean offset of 2.2 m. Considering the factors discussed above, and the lack of offset shown by the Halifax data to which a tidal correction was able to be applied, it seems likely that the exhibited depth offset compared with the survey data at chart datum is not an artefact of the radar analysis but largely the result of a combination of predicted and meteorological tide. It should be noted that the Halifax data exhibited a tidal offset of 2.3 m that was determined independently from the radar data, so the offset of 2.2 m between the radar and survey data during the St Margaret's Bay trial is within a reasonable range for that general region and conditions.

The comparison of the results in Fig. 16 shows the offset clearly, and there is also more scatter to the data than in the Halifax trial as exhibited by the lower correlation coefficient of R=0.8, R^2=0.71. This is perhaps to be expected

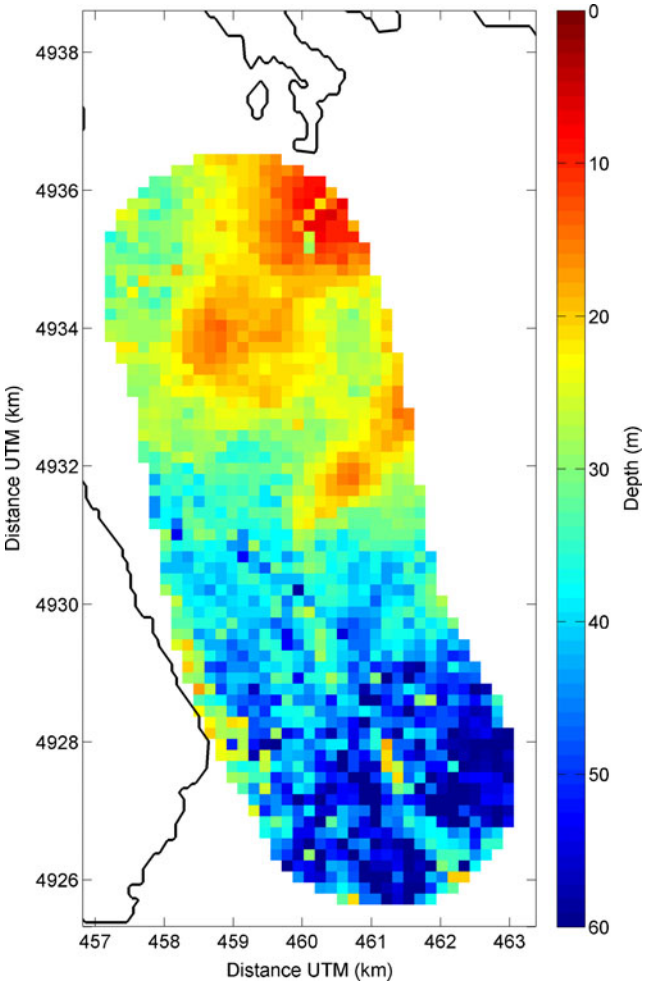

Fig. 11 The radar-derived bathymetry determined from approximately 20 min of data collected from the CFAV Quest travelling at 10–14 knots

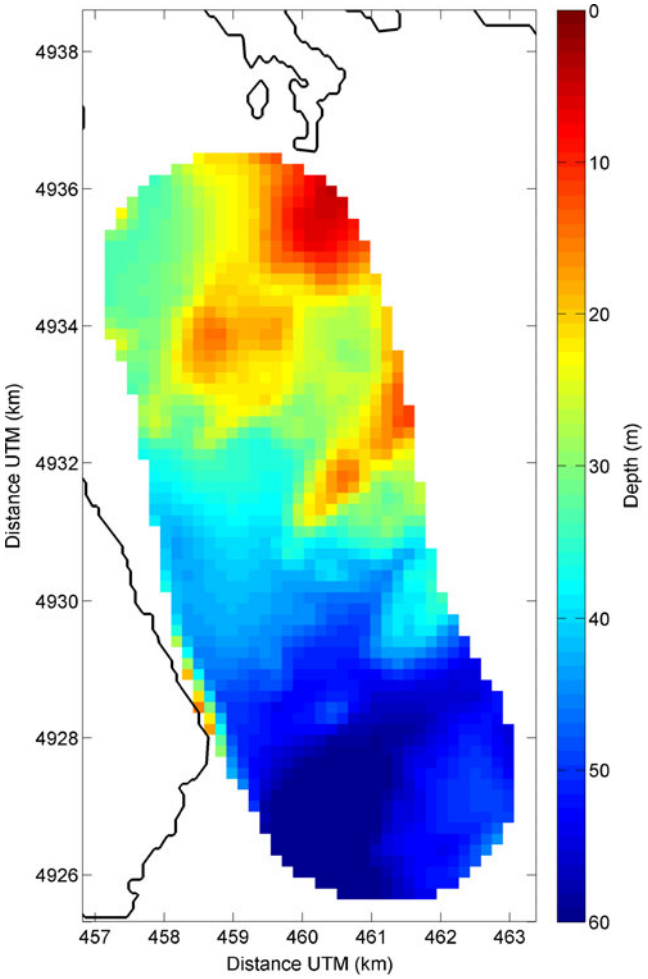

Fig. 12 Gridded survey data with a tide level added that was determined from the difference between the ship's echosounder and the survey

considering the variability observed between the Quest's echo sounder and the survey, the variation in topography over the study area and the longer time taken to record the data. The bottoming out effect is much clearer in these results, with an evident levelling off of the radar-derived water depths in waters deeper than 50 m as the waves cease to respond to the sea bed in a measurable fashion.

Nonetheless, the qualitative correlation between the survey and the radar-derived bathymetry is evident and the technique was able to map approximately 64 km^2 of coastal seas within a bay using data that took 2 h to collect during a moderate wave event and using equipment already available on the ship.

6 Conclusions

It has been clearly demonstrated that the use of radar data recorded from a moving vessel may be used as the source

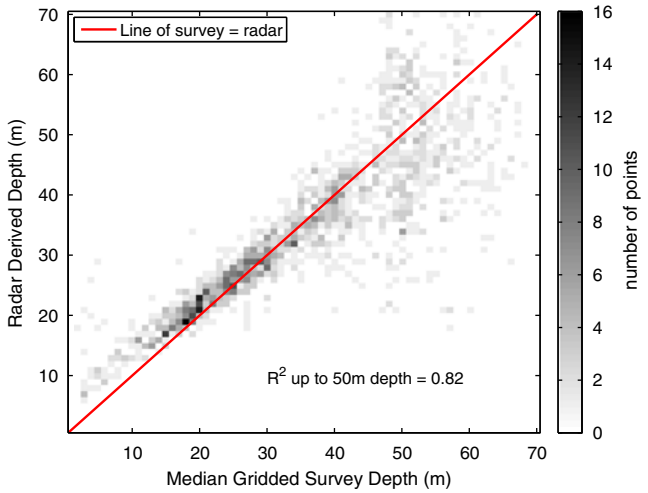

Fig. 13 A comparison of the results from the Halifax radar depth inversion and the survey data with a mean tidal level of 2.3 m added

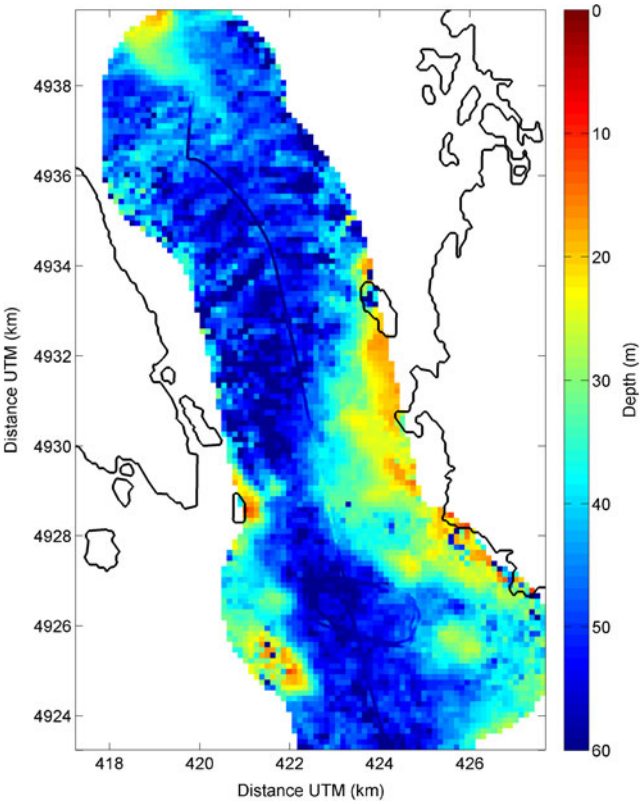

Fig. 14 The radar-derived bathymetry determined from 2 h of data collected from the CFAV Quest travelling slowly through St Margaret's Bay. The echosounder record from the CFAV Quest has been overlaid as a *solid line colour* coded with the measured depth

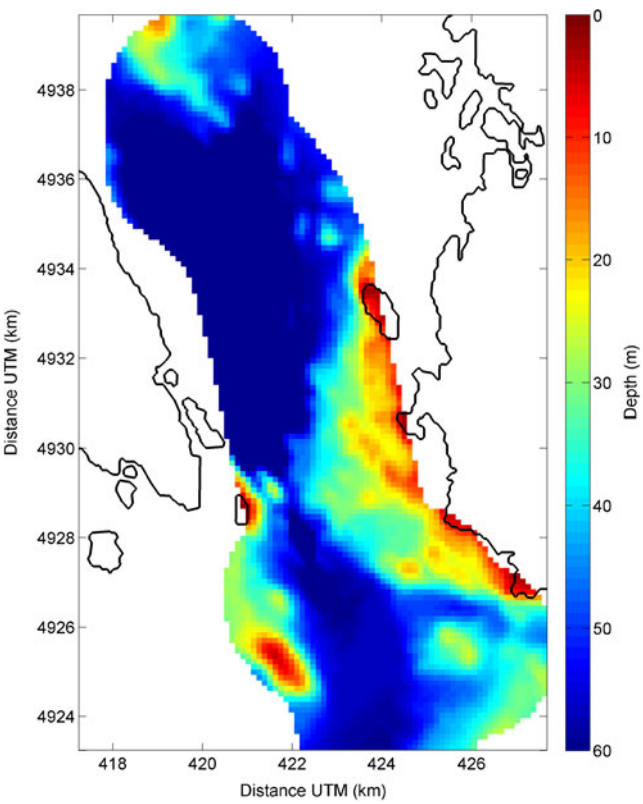

Fig. 15 Gridded survey data with no tide level added, so the depth will appear artificially shallower than the actual water depths at the time of the trial

data for depth inversion analyses, given sufficiently accurate georeferencing data for each radar image within the images sequences. The depths that can be determined are limited by the wave periods present at the time and have been shown to be consistent with a general rule of thumb that the maximum applicable depth is related to around a quarter of the wavelength of the waves, corresponding to waves with wavelengths approximately 90% of the deep-water wavelength.

The lack of coherent wave patterns for wave periods much below 8 s following spectral analyses of the georeferenced image sequences suggests that further improvements in the georeferencing could improve the quality of future results significantly and may permit the determination of currents from the higher frequency components if they are able to be adequately resolved.

The technology already exists for high frequency position and bearing fixes to be recorded at rates of tens to hundreds of times per second, which would make possible the accurate georeferencing of each radar pulse return, thereby removing these positioning errors and allowing full depth and current inversions to a quality equal to that possible from radars mounted on static platforms.

This paper has demonstrated what is possible with standard ship's navigation data in terms of depth mapping. In the near future, it is quite likely the necessary processing could be performed in near real time thereby allowing ships

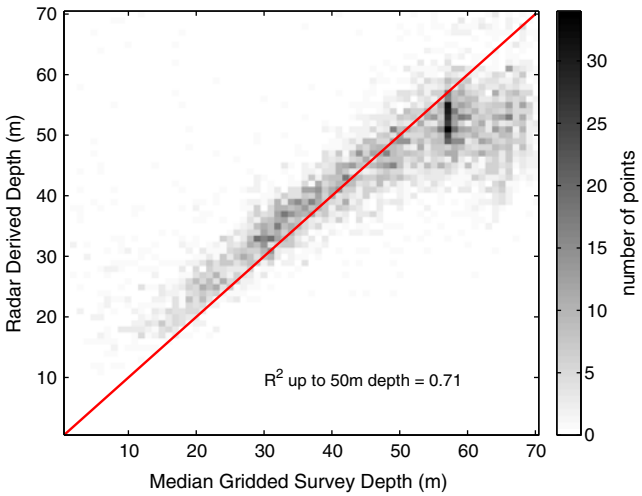

Fig. 16 A comparison of the results from the St Margaret's Bay radar depth inversion and the survey data. The survey was not corrected for the tidal level, so the clear offset in the data of 2.2 m is thought to be the combination of predicted and meteorological tide

to map the depths and currents some kilometres ahead and in areas the vessels themselves would not be able to enter.

Acknowledgements The authors wish to thank Doug Caldwell and Meng-Han Chi at DRDC Atlantic, and Bob MacDonald and the crew of the CFAV Quest for collecting the radar data and providing access to the CFAV Quest navigation data.

References

Aarninkhof SGJ, Ruessink BG, Roelvink JA (2005). Nearshore subtidal bathymetry from time-exposure video images. Journal of Geophysical Research, 110, C06011, doi:10.1029/2004JC002791

Airy GB (1845) "Tides and waves". Encyclopaedia Metropolitana

Bacon Sir R (1932) "The concise story of the Dover Patrol". London

Banerjee D (2006) PLL performance, simulation and design handbook (4th ed.), National Semiconductor

Bell PS (1999) Shallow water bathymetry derived from an analysis of X-band marine radar images of waves. Coast Eng 37:513–527

Bell PS (2008) Mapping shallow water coastal areas using a standard marine x-band radar. In: Hydro8, Liverpool, 4th-6th November 2008. Liverpool, International Federation of Hydrographic Societies

Bell PS (2009) Remote bathymetry and current mapping around shore-parallel breakwaters. Proceedings of 33rd International Association of Hydraulic Engineering & Research (IAHR) Biennial Congress, Vancouver, Canada, August 9–14, 2009

Bell PS (2010) Submerged dunes and breakwater embayments mapped using wave inversions of shore-mounted marine X-band radar data. IEEE International Geoscience & Remote Sensing Symposium July 25–30, 2010, Honolulu, Hawaii, U.S. A., ISBN: 978-1-4244-9564-1, Paper FR3-L02.3, 4334-4337

Bell PS, Williams JJ, Clark S, Morris BD, Vila Concejo A (2006) Nested radar systems for remote coastal observations. J Coast Res SI 39:483–487

Bendat JS, Piersol AG (1971) Random data: analysis and measurement procedures. Wiley, ISBN 0-471-06470-X

Booij N (1981) "Gravity waves on water with non-uniform depth and current". Rep. No.81-1, Dept. Civ. Eng., Delft University of Technology

Catalan PA, Haller MC (2008) Remote sensing of breaking wave phase speeds with application to non-linear depth inversions. Coast Eng 55:93–111

Dugan JP, Piotrowski CC, Williams JZ (2001) Water depth and surface current retrievals from airborne optical measurements of surface gravity wave dispersion. J Geophys Res 106(C8):16,903–16,915

Flampouris S, Ziemer F, Seemann J (2008) Accuracy of bathymetric assessment by locally analyzing radar ocean wave imagery. IEEE Trans Geosci Remote Sens 46(10):2906–2913. doi:10.1109/TGRS.2008.919687, part1

Hart CA, Miskin EA (1945) "Developments in the method of determination of beach gradients by wave velocities". Air survey research paper no. 15, Directorate of Military Survey, UK War Office

Heathershaw AD, Blackley MWL, Hardcastle PJ (1980) Wave direction estimates in coastal waters using radar. Coast Eng 3:249–267

Hedges TS (1976) An empirical modification to linear wave theory. Proc Inst Civ Eng 61:575–579

Hedges TS (1987) Discussion: an approximate model for nonlinear dispersion in monochromatic wave propagation models, by J.T. Kirby and R.A. Dalrymple. Coastal Eng 11:87–89

Hessner K, Reichert K, Rosenthal W (1999) "Mapping of sea bottom topography in shallow seas by using a nautical radar," 2nd Symposium on Operationalization of Remote Sensing, ITC, Enschede, Netherlands, 16-20 August 1999

Hessner K, Nieto Borge JC, Bell PS (2008) "Nautical Radar Measurements in Europe - Applications of WaMoS II", in Remote Sensing of the European Seas. Ed.: V. Barale, and M. Gade. Publisher: Springer. ISBN: 978-1-4020-6771-6

Hill RJ (2005) "Motion compensation for shipborne radars and lidars". NOAA Technical Memorandum OAR PSD 309

Holland TK (2001) Application of the linear dispersion relation with respect to depth inversion and remotely sensed imagery. IEEE Trans Geosci Remote Sens 39(11):2060–2071

Kirby JT, Dalrymple RA (1986) An approximate model for nonlinear dispersion in monochromatic wave propagation models. Coastal Eng 9:545–561

Kirby JT, Dalrymple RA (1987) Discussion reply: an approximate model for nonlinear dispersion in monochromatic wave propagation models. Coastal Eng 11:89–92

Reichert K, Borge JCN, Dittmer J (1998) "WaMoS II: an operational wave monitoring system". Proceedings of Oceanology International 98: The Global Ocean, 10-13 March 1998, Brighton, UK, 3, 455-462

Ruessink BG, Bell PS, van Enckevort IMJ, Aarninkhof SGJ (2002) Nearshore bar crest location quantified from time-averaged Xband radar images. Coastal Eng 45:19–32. doi:10.1016/S0378-3839(01)00042-4

Senet CM, Seemann J, Ziemer F (2001) The near-surface current velocity determined from image sequences of the sea surface. IEEE Trans Geosci Remote Sens 39(3):492–505

Senet CM, Seemann J, Flampouris S, Ziemer F (2008) Determination of bathymetric and current maps by the method DiSC based on the analysis of nautical X-Band radar image sequences of the sea surface. IEEE Trans Geosci Remote Sens 46(8):2267–2279. doi:10.1109/TGRS.2008.916474

Takewaka S (2005) Measurements of shoreline positions and intertidal foreshore slopes with Xband marine radar system. Coast Eng J JSCE 47:91–107

Williams WW (1946) "The determination of gradients on enemy-held beaches". Geogr J XIC, 76-93

Young IR, Rosenthal W, Ziemer F (1985) A three-dimensional analysis of marine radar images for the determination of ocean wave directionality and surface currents. J Geophysical Research 90 (C1):1049–1059